Rab32 Modulates Apoptosis Onset and Mitochondria-associated Membrane (MAM) Properties[*]

Michael Bui[‡], **Susanna Y. Gilady**[‡], **Ross E. B. Fitzsimmons**[‡], **Matthew D. Benson**[‡1], **Emily M. Lynes**[‡1], **Kevin Gesson**[‡], **Neal M. Alto**[§], **Stefan Strack**[¶], **John D. Scott**[‖], and **Thomas Simmen**[‡2]

From the [‡]*Department of Cell Biology, School of Molecular and Systems Medicine, University of Alberta, Edmonton, Alberta T6G 2H7, Canada, the* [§]*Department of Microbiology, University of Texas Southwestern, Dallas, Texas 75390, the* [‖]*Department of Pharmacology, School of Medicine, University of Washington, Seattle, Washington 98195-7280, and the* [¶]*Department of Pharmacology, University of Iowa Carver College of Medicine, Iowa City, Iowa 52242*

The mitochondria-associated membrane (MAM) has emerged as an endoplasmic reticulum (ER) signaling hub that accommodates ER chaperones, including the lectin calnexin. At the MAM, these chaperones control ER homeostasis but also play a role in the onset of ER stress-mediated apoptosis, likely through the modulation of ER calcium signaling. These opposing roles of MAM-localized chaperones suggest the existence of mechanisms that regulate the composition and the properties of ER membrane domains. Our results now show that the GTPase Rab32 localizes to the ER and mitochondria, and we identify this protein as a regulator of MAM properties. Consistent with such a role, Rab32 modulates ER calcium handling and disrupts the specific enrichment of calnexin on the MAM, while not affecting the ER distribution of protein-disulfide isomerase and mitofusin-2. Furthermore, Rab32 determines the targeting of PKA to mitochondrial and ER membranes and through its overexpression or inactivation increases the phosphorylation of Bad and of Drp1. Through a combination of its functions as a PKA-anchoring protein and a regulator of MAM properties, the activity and expression level of Rab32 determine the speed of apoptosis onset.

Mitochondria are in extensive contact with the secretory pathway. Mostly, these contacts occur on a domain of the endoplasmic reticulum (ER)[3] called the mitochondria-associated membrane (MAM) (1). This specialized region of the ER has recently been the subject of much interest as a major cellular signaling hub (2–5). Signaling on the MAM utilizes direct calcium transfer between the ER and mitochondria (6–8). Effi-

cient import of calcium into the ER keeps chaperones functional and avoids the accumulation of unfolded proteins, a condition called ER stress (9), but conversely, the rapid calcium efflux from the ER and its transfer to mitochondria following ER stress triggers apoptosis (10–12). Likewise, mitochondrial metabolism benefits from increased calcium by an increase in NADH production from pyruvate, α-ketoglutarate, and isocitrate dehydrogenases, but calcium overload results in massive production of reactive oxygen species and a loss of mitochondrial membrane potential (13). Therefore, ER calcium handling on the MAM acts as a double-edged sword, suggesting that as yet unknown regulatory mechanisms decide between its pro-homeostatic or pro-apoptotic role. One such regulatory mechanism may depend on the amount of ER chaperones that localize to the MAM (2, 4). ER chaperones and oxidoreductases associate reversibly with calcium channels and pumps dependent on redox and calcium conditions, thereby regulating ER-mitochondrial calcium flux (14–17). For instance, ER stress triggers the induction of the oxidoreductase Ero1α, which then stimulates inositol 1,4,5-triphosphate receptor activity on the MAM, possibly by modulating the ER luminal redox environment (18, 19). Conversely, the MAM-enriched lectin calnexin attenuates calcium oscillations by interacting with sarcoplasmic/endoplasmic reticulum calcium ATPase (SERCA) 2b (2, 15). Thus, ER oxidative protein folding appears to determine the properties of the MAM, a function that may explain the increased apposition between the ER and mitochondria upon ER stress (20). In line with these findings, a disruption of MAM results in a reduced folding capacity of the ER, concomitant with ER stress (12, 21, 22).

Although searches for MAM forming factors have led to identification of a tethering complex termed ERMES in yeast (23, 24) and of Grp75 and mitofusin-2 in mammalian cells (5, 25), not a lot is known about proteins mediating the enrichment of ER proteins on the MAM. Insight into how the ER establishes its domains would, however, help our understanding of the functioning of the MAM and other domains of the ER. Our laboratory has so far identified one such mechanism in the form of the cytosolic phosphofurin acidic cluster sorting protein 2 (PACS-2) (2, 12). PACS-2, like other MAM targeting factors to be characterized, influences the properties of the MAM by regulating its composition and impacts on MAM formation as well. Through these functions, PACS-2 is an important regulator of apoptosis onset (12, 26, 27).

[3] The abbreviations used are: ER, endoplasmic reticulum; MAM, mitochondria-associated membrane; SERCA, sarcoplasmic/endoplasmic reticulum calcium ATPase; AKAP, cAMP-dependent protein kinase-anchoring protein; PDI, protein disulfide isomerase; TRAIL, tumor necrosis factor-related apoptosis-inducing ligand; rER, rough ER.

Interestingly, PACS-2 knockdown does not completely abolish MAM targeting of calnexin, an ER chaperone that is enriched on the MAM (2). This finding indicates the existence of other proteins implicated in the MAM domain establishment. Because Rab proteins regulate homotypic fusion of ER tubules (28), candidates for such proteins could be found among this extensive protein family. Members of these Ras-related small GTPases direct intracellular vesicular traffic (29, 30) but also regulate the structure of the ER and its apposition to other organelles. Specifically, Rab5 modulates the morphology of the peripheral ER, whereas Rab18 promotes the apposition of the ER to lipid droplets (31, 32). Furthermore, the yeast Rab Ypt11 determines the spatial distribution of mitochondria and their inheritance (33). When searching for Rab proteins that are candidate regulators of MAM formation and targeting, we focused on Rab32, because it is thought to be enriched on mitochondria (34).

Its localization is not the only characteristic that distinguishes Rab32 from other Rabs. Human Rab32 is also the only known Rab protein that can function as a cAMP-dependent protein kinase (PKA)-anchoring protein (AKAP) (35, 36). This group of proteins allows PKA to phosphorylate substrates locally rather than globally (37). For instance, the mitochondrial AKAP121 assembles a PKA and Src-containing signaling complex on mitochondria, leading to enhanced mitochondrial metabolism and the phosphorylation of the PKA substrate Bad, concomitant with a block in apoptosis (38, 39). Our results now show that endogenous and overexpressed Rab32 localizes to mitochondria and the MAM in HeLa cells. Consistent with this dual localization to the ER and mitochondria and its identity as an AKAP, we found that Rab32 modulates MAM properties and apoptosis onset.

EXPERIMENTAL PROCEDURES

Antibodies and Reagents—All chemicals were from Sigma, except for H89 (Axxora, San Diego). The Rab32 and Rab32 mutant expressing plasmids and the rabbit anti-Rab32 antiserum have been described previously (34). The anti-phospho Drp1 has been described (40). The rabbit anti-calnexin antiserum was generated using a cytosolic peptide by Open Biosystems, Huntsville, AL. Antibodies against GAPDH and MPR46 were provided by Tom Hobman, Edmonton, Alberta, Canada. Antibodies to Sec23 (Abcam, Cambridge, UK), PDI, Drp1, ACAT1 (Thermo, Golden, CO), caspase-3, caspase-8, phospho-Bad serine 112 and 136 (Cell Signaling, Danvers, MA), β-tubulin (Calbiochem), mitochondrial complex 2 (Mitosciences, Eugene, OR), Mitofusin-1 (Abnova, Taipeh, Taiwan), Mitofusin-2 (Sigma), PKA RII (Santa Cruz Biotechnology, Santa Cruz, CA), FLAG tag, Bad, phospho-Bad serine 155 (Millipore, Billerica, MA) were purchased as indicated. HeLa cells were from ECACC (Porton Down, UK) and cultured in DMEM (Invitrogen) containing 10% fetal bovine serum (Invitrogen). Human Rab32 siRNAs (HSS116975) were from Invitrogen. TRAIL was from Millipore (Billerica, MA). The AnnexinV/PI kit was from Calbiochem.

Immunofluorescence Microscopy, Transfections, Western Blotting—Processing for immunofluorescence microscopy was performed as follows. HeLa cells were grown on coverslips for

24 (untransfected cells) or 48 h (when plasmid- or siRNA-transfected). Cells were washed with PBS containing 1 mM CaCl$_2$ and 0.5 mM MgCl$_2$ (PBS++) and fixed with 4% paraformaldehyde for 20 min. After washing with PBS++, cells were permeabilized for 1 min with 0.1% Triton X-100, 0.2% BSA in PBS++. Cells were then incubated with primary antibodies (1:100) and secondary antibodies in PBS++, 0.2% BSA for 1 h each, interrupted with three washes using PBS++. All secondary antibodies were AlexaFluor-conjugated 350, 488, or 546 (Invitrogen) used at 1:2,000. Samples were mounted in Prolong AntiFade (Invitrogen). Images were obtained with an Axiocam on an Axio Observer microscope (Carl Zeiss, Jena, Germany) using a 100× plan-Apochromat lens. All images were iteratively deconvolved using the Axiovision 4 software. Deconvolved images were enhanced with Photoshop (Adobe, San Jose, CA) using the levels functions only, until reaching saturation in the most intense areas of the image. Transfections were done using MetafectenePRO (Biontex, Martinsried, Germany), according to the manufacturer's instructions. Western blotting procedures were done according to standard protocols using goat-anti mouse/rabbit secondary antibodies conjugated to Alexafluor 680/750 (Invitrogen) on an Odyssey infrared imaging system (LICOR, Lincoln, NE).

Membrane Fractionation, Protein-Protein Binding, and Biotinylation Assays—Mitochondria and light membranes were separated as described previously (12). The MAM OptiPrep™ gradient protocol was described previously (2). Mitochondria were separated from the MAM as follows; HeLa cells were grown to confluency on 15 20-cm dishes and homogenized using a ball-bearing homogenizer as above in 4 ml of isolation buffer (250 mM mannitol, 5 mM HEPES, pH 7.4, 0.5 mM EGTA, 0.1% BSA). Debris and nuclei were removed by 5 min of centrifugation at 600 × g in 15-ml Corex tubes in a JA-20 rotor. The supernatant was centrifuged at 8,500 rpm in a JA-12 rotor for 10 min to pellet crude mitochondria. Subsequently, microsomes were pelleted at 100,000 × g for 1 h in a TLA120.2 rotor. The previously isolated mitochondria were resuspended in 1 ml of isolation medium and layered on top of 8.5 ml of Percoll isolation medium (225 mM D-mannitol, 25 mM HEPES, pH 7.4, 1 mM EGTA and 20% Percoll (v/v)) in a 10-ml Ultraclear polycarbonate Beckman tube. The tube was centrifuged for 30 min at 30,500 rpm (95,000 × g) in a Ti-70 rotor with slow acceleration and deceleration, after which purified mitochondria (¾ down the tube) and MAM were removed from the Percoll gradient (located above the mitochondria). Percoll was removed from the mitochondrial fraction, and the MAM fraction was diluted 5-fold with fresh isolation medium and re-centrifuged at 60,000 rpm in a TLA120.2 rotor for 1 h. Equal proportional amounts were loaded for all fractions.

Calcium Measurements—ER calcium handling was measured on HeLa cells transfected as indicated and loaded with 2 μM FURA-2 (Invitrogen). 2 × 10^6 cells were trypsinized and resuspended in DMEM, 10% fetal bovine serum. Cells were pelleted at 800 rpm and resuspended in 2 ml of Tyrode's buffer (2.5 mM KCl, 135 mM NaCl, 10 mM glucose, 1 mM MgCl$_2$, 1 mM CaCl$_2$, pH 7.4). Cell suspensions were monitored for light emission at 510 nm after excitation at 340 and 380 nm on an 814 photomultiplier detection system (PTI, Birmingham, NJ). Cal-
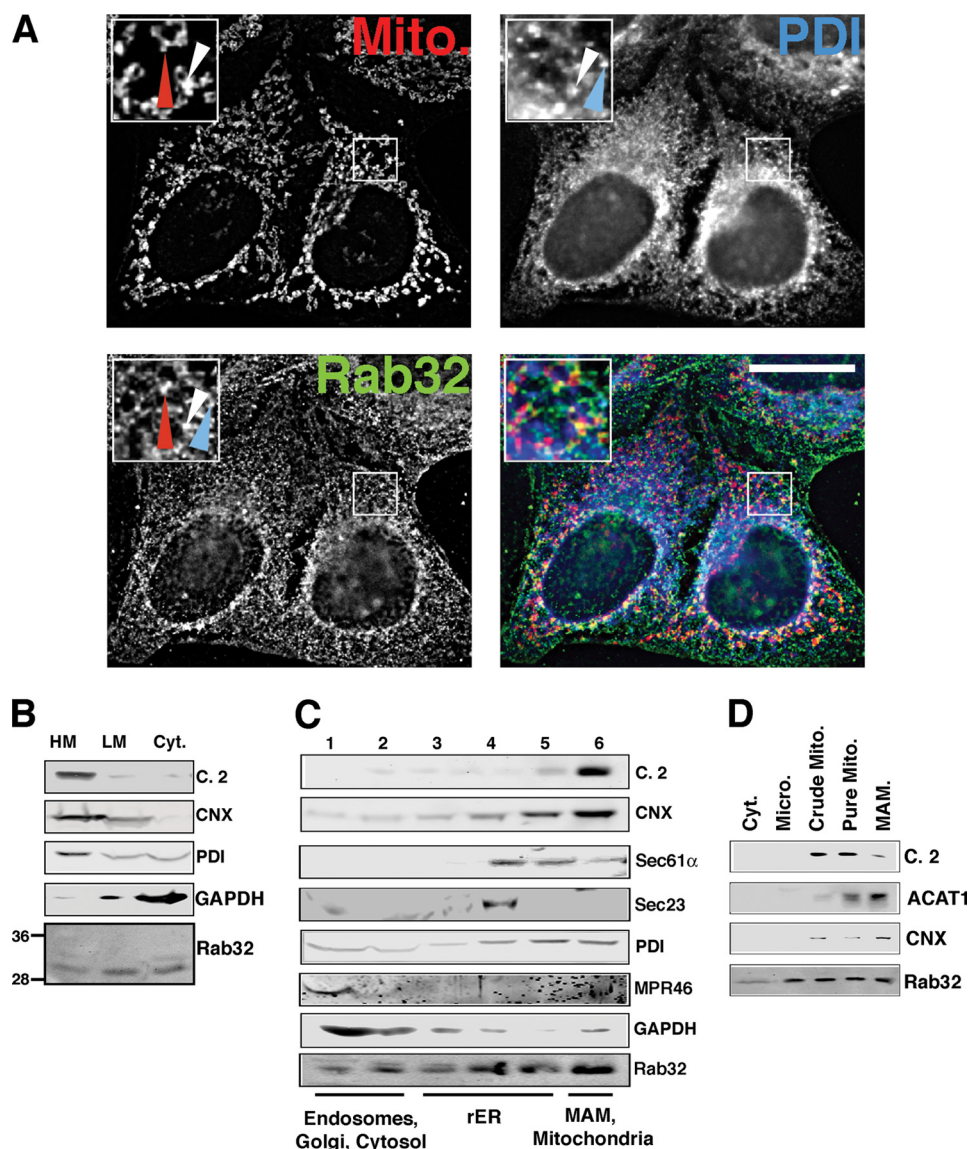
FIGURE 1. **Intracellular localization of Rab32.** *A,* a portion of Rab32 colocalizes with the ER. HeLa cells were grown on coverslips for 24 h and processed for immunofluorescence microscopy. Rab32 was detected with our rabbit polyclonal antibody and PDI with a mouse monoclonal antiserum (ABR, Golden, CO), and mitochondria (*Mito*) were preloaded with MitoTracker. *Insets* show a magnified area, indicated by *white frames* on the bigger pictures. The *red arrowheads* point out Rab32/mitochondria overlap, and the *blue arrowheads* point out Rab32/PDI overlap. An example of triple overlap is highlighted by *white arrowheads*. *Scale bar,* 25 μm. *B,* Rab32 fractionation into heavy (*HM*) and light membranes (*LM*) and the cytosol (*Cyt*). Membranes from HeLa cells were fractionated into low and high speed pellets, which were analyzed by Western blot for complex II (mitochondria), calnexin (ER/MAM), PDI (all ER), GAPDH (cytosol), and Rab32 (with molecular masses in kDa are indicated on the *left*). *C,* Rab32 distribution upon ER domain fractionation. HeLa cell homogenates were fractionated on a discontinuous 10–30% OptiPrep™ gradient. Marker proteins indicate mitochondria (complex II), MAM (calnexin), rER (Sec61α), transitional ER (Sec23), pan-ER (PDI), endosomes (MPR46), and cytosol (GAPDH). Fractions are assigned their predominant content. *D,* Rab32 distribution between mitochondria (*Mito*) and the MAM. HeLa cell homogenates were fractionated according to "Experimental Procedures." Marker proteins indicate mitochondria (complex 2, *C.2*) and the MAM (acyl-CoA:cholesterol acyltransferase 1, ACAT1, and calnexin, *CNX*). *Micro*, microsomes.

cium release was triggered by the addition of 200 μM histamine, whereas the inhibition of SERCA was achieved with the addition of 1 μM thapsigargin.

RESULTS

Rab32 Localizes to the ER and Mitochondria—Rab32 is a small GTPase that is ubiquitous in mammals and whose highest expression levels are found in liver, heart, spleen, and testis (41,

42). In skin, it appears to play a role in melanocyte biogenesis (43, 44). However, its trafficking properties have so far not been addressed in cells that lack melanosomes. Because HeLa cells are a well accepted model system to study intracellular trafficking and apoptosis onset, we decided to investigate the localization and function of Rab32 in these cells. We processed HeLa cells for immunofluorescence microscopy and incubated them with antibodies against endogenous Rab32. We detected a punctate staining pattern that appeared like a composite of ER and mitochondria (Fig. 1*A*). As a marker for the ER, we used the oxidoreductase PDI, which is found in all domains of the ER (see below). When analyzing the Rab32 staining pattern, we found that Rab32 showed considerable overlap with MitoTracker as published (Fig. 1*A*, *red arrowheads*) (34), but it was also found on spots that were exclusively labeled with anti-PDI antibodies (Fig. 1*A*, *blue arrowheads*). Interestingly, several spots of Rab32 staining co-labeled with PDI and MitoTracker (Fig. 1*A*, *white arrowheads*). To determine which part of the ER was enriched with Rab32, we subjected cellular homogenates to various subcellular fractionation protocols designed to answer the distribution of Rab32 between the cytosol and ER and mitochondrial membranes (Fig. 1*B*), on domains of the ER (Fig. 1*C*), and between mitochondria and the MAM (Fig. 1*D*). First, we separated cellular membranes into cytosol and heavy and light membranes to determine the extent of Rab32 membrane association. Although the majority of endogenous Rab32 was membrane-associated, roughly one-third was found in the cytosol (Fig. 1*B*).

To further examine the localization of Rab32, we analyzed its distribution along the secretory pathway and on domains of the ER using a 10–30% OptiPrep™ gradient protocol. With this method, we can routinely determine whether an ER protein is found leaking to the late secretory pathway, or resides on the rough ER (rER) or on the MAM; on our Optiprep gradients, endosomal proteins peak at the top of this gradient (MPR46), rER proteins peak in the middle fractions 3–5 (Sec61α), and

MAM proteins co-peak with mitochondrial markers at the bottom in fraction 6 (calnexin) (2). To ease detection of rare proteins, we split this gradient into six fractions. This protocol allowed us to detect significant overlap of Rab32 with the endosomal mannose 6-phosphate receptor (MPR46) and cytosolic GAPDH (Fig. 1C) in fractions 1 and 2, but we also noticed considerable amounts of Rab32 co-migrating with the transitional ER marker Sec23 in fraction 4, the rER marker Sec61α in fractions 4 and 5, and the mitochondrial complex 2 in fraction 6 (Fig. 1C). Because the OptiPrep™ protocol can distinguish between rER and MAM, but not between MAM and mitochondria, we also separated ER and mitochondrial membranes of HeLa cells on a Percoll gradient (1, 45). With this protocol, we detected Rab32 on microsomes, mitochondria, and the MAM (Fig. 1D). Therefore, our immunofluorescence analysis and our three fractionation protocols consistently detect endogenous Rab32 in the cytosol, on mitochondria, and on the MAM of HeLa cells, in addition to lesser amounts on membranes of the late secretory pathway as documented previously for overexpressed GFP-tagged Rab32 (43, 44).

Active and Inactive Rab32 Localize to Distinct Intracellular Membranes—Next, we decided to express and analyze FLAG-tagged Rab32 wild type and Rab32 mutants that preferentially bind to GDP (T39N, dominant-negative) or GTP (Q85L, dominant-active) in HeLa cells, to determine whether it is active or inactive Rab32 that shows preferential association with mitochondria and the MAM. Wild type Rab32 co-localized very nicely with the MAM-enriched ER marker calnexin but also showed some overlap with mitochondria (Fig. 2A). The dominant-active Q85L mutant still co-localized with calnexin, but it showed more cytosolic staining than wild type Rab32 and did not exhibit any significant overlap with mitochondria (Fig. 2B). In contrast, the T39N dominant-negative mutant showed some overlap with both mitochondria and the ER, but it also caused the clustering of mitochondria close to the nucleus, as published previously (Fig. 2C) (34). These results suggested that GTP-bound Q85L and GDP-bound T39N might have opposing distributions in terms of their overlap with mitochondria. To test for that possibility, we first fractionated homogenates of Rab32-transfected cells into cytosol and heavy and light membranes and probed for Rab32 constructs (Fig. 2D). The membrane-associated moiety of Rab32Q85L that fractionated with heavy membranes was significantly lower than for either wild type or T39N Rab32 (46% *versus* 65 and 71%, respectively). Therefore, this protocol confirmed our immunofluorescence microscopy findings, because heavy membranes contain MAM and mitochondrial markers (Fig. 1B). Using our OptiPrep™ protocol, we confirmed further that Rab32Q85L preferentially co-fractionates with peripheral membranes, whereas Rab32T39N co-fractionates with perinuclear membranes of the ER and mitochondria (Fig. 2E). The amount of endogenous Rab32 and Rab32T39N found at the bottom of our gradient in fractions 5 and 6 amounted to around 50% of total, whereas only about 35% of overexpressed wild type Rab32 and about 20% of Rab32Q85L associated with these fractions. Given the bipartite localization of Rab32 to the ER and mitochondria and the opposing distributions of GDP and GTP-bound Rab32 along the secretory

pathway, we therefore hypothesized that Rab32 could be involved in cargo targeting to the mitochondria or the MAM.

Rab32 Controls the Intracellular PKA Distribution and Signaling—To examine a role of Rab32 in intracellular cargo distribution on the MAM and mitochondria, we chose to first focus on PKA and its substrates, because this kinase signals from mitochondria and is a known interactor of Rab32 (34). Previously, overexpressed GFP-tagged Rab32 had been shown to recruit PKA RIIα to melanosomes, a function that is important for melanosome biogenesis (44). However, because membrane-bound endogenous Rab32 localizes predominantly to the ER and mitochondria in HeLa cells that lack melanosomes (Fig. 1, C and D), we hypothesized that the AKAP function of Rab32 could go beyond melanosome biogenesis and could extend to mitochondria. We first examined the intracellular localization of PKA RIIα in control cells and cells expressing wild type Rab32 and its mutants. We found that increased amounts of Rab32 led to an increased association of PKA with ER membranes that overlapped partially with mitochondria (Fig. 3A). Similarly, the expression of a GDP-bound Rab32 led to the increased association of Rab32 with heavy membranes, concomitant with mitochondrial fusion, typical for this construct (Fig. 3, A and B). This relocation of PKA coincided with increased amounts of PKA on heavy membranes that contain mitochondria and the MAM (Fig. 3B). Conversely, we saw opposite effects with a GTP-bound Rab32 mutant that led to an increased association of PKA with light membranes, and a reduction of PKA on membranes of the MAM and mitochondria (Fig. 3B). The expression of a Rab32 mutant that is not able to bind to PKA resulted in a marked reduction of membrane-bound PKA, in particular on light membranes, and in a relocation of PKA to the cytosol. This was evident by immunofluorescence and fractionation. Overexpression levels *versus* endogenous Rab32 were in the order of 2–4-fold (Fig. 3C). Together, our results demonstrate that the AKAP characteristics and the GTPase activity of Rab32 determines PKA targeting to heavy membranes and the MAM, leading us to hypothesize that Rab32 alters mitochondrial PKA signaling.

Thus, we first tested this hypothesis by analyzing the individual phosphorylation status of the Bcl2 family protein Bad, given the precedent of AKAP121 regulating the phosphorylation state of Bad on mitochondria (46). Our results show that the overexpression of Rab32 wild type and Rab32 T39N roughly doubled the phosphorylation of Bad on the human equivalent PKA site of mouse Bad serine 155 (serine 118), consistent with their ability to lead to increased targeting of PKA RIIα to heavy membranes (Fig. 3C). Both the activation of Rab32 (Rab32Q85L) and the expression of a Rab32 mutant that is not able to promote PKA RIIα localization to cellular membranes did not affect Bad serine 155 levels but led to decreases in Bad phosphorylation on serine 136 that is a preferred substrate of Akt (Fig. 3C) (47). One explanation for these changes could lie in an alteration of Bad targeting. However, our results show that this was not the case regardless of the activity and expression level of Rab32 (Fig. 3D). Because PKA mediates Bad phosphorylation on serine 155, we also determined the localization of Bad Ser(P)-155 (48). Under all conditions, the

amounts of Bad that were phosphorylated on serine 155 were mostly associated with heavy membranes, suggesting that Rab32 does not influence the localization of PKA-phosphorylated Bad (Fig. 3*D*). Together, our results suggest that Rab32 dictates the extent of Bad PKA phosphorylation on serine 155 but not its localization.

To further investigate the hypothesis that Rab32 modulates PKA signaling on mitochondria and impacts the Bad phosphorylation state, we depleted Rab32 using siRNA. Again, we tested whether Rab32 expression levels affected the localization of PKA RIIα. Contrary to the overexpression of wild type Rab32, we detected a loss of PKA RIIα on heavy membranes
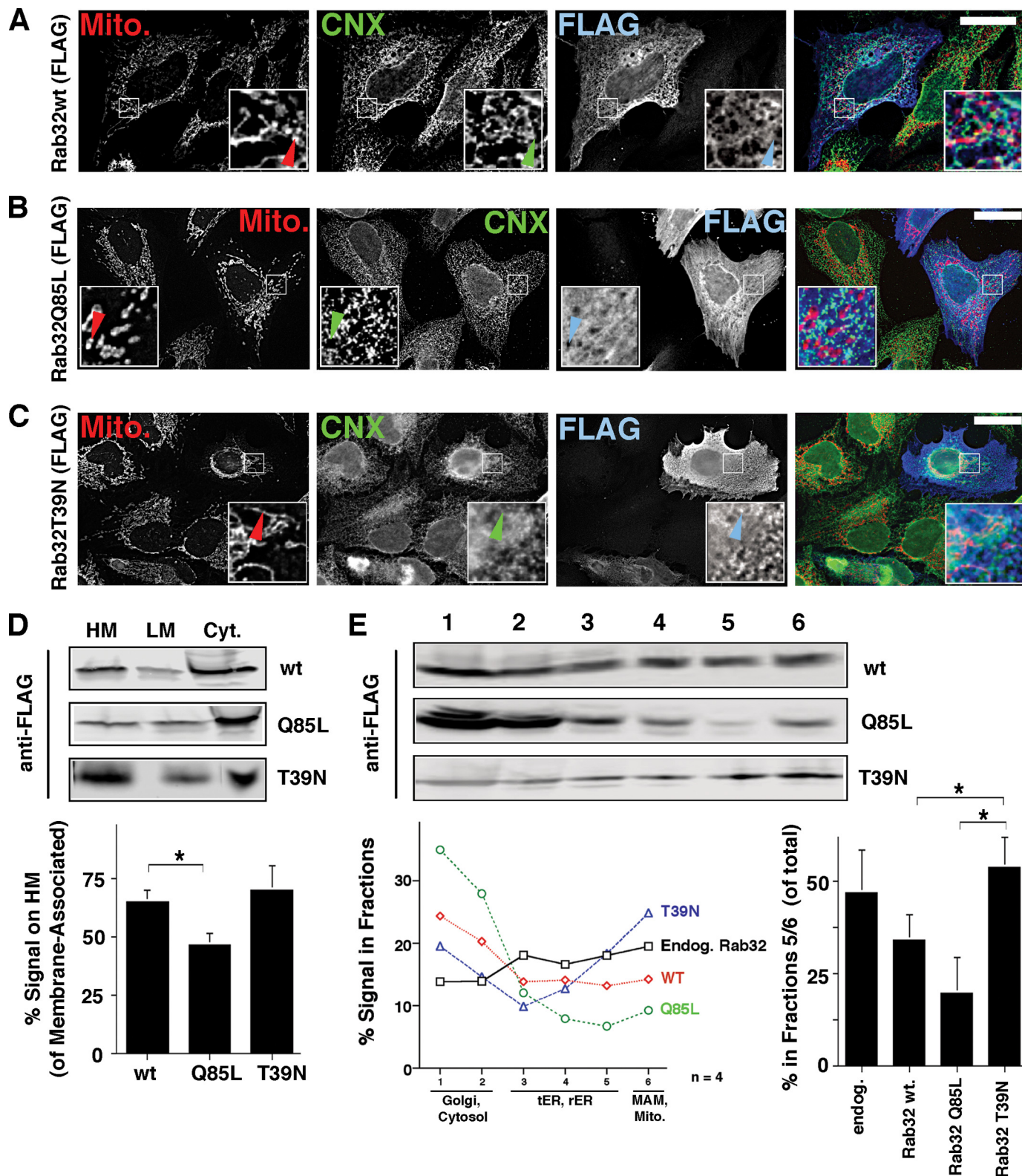
and a reduction of the PKA RIIα overlap with mitochondria (Fig. 3*E*). This effect resulted in reduced Bad phosphorylation on serine 155 (Fig. 3*E*), but like Rab32 overexpression, Rab32 knockdown does not affect other Bad phosphorylation sites (Fig. 3, *B* and *E*). Together, our results demonstrate that Rab32 determines the association of PKA with the MAM and mitochondria and thus modulates Bad phosphorylation on serine 155. In addition, the activation of Rab32 also decreases phosphorylation of Bad on serine 136. We evaluate the effects and consequences of this interference further below and under the "Discussion."

Next, we aimed to test whether other mitochondrial PKA substrates are also under the influence of Rab32. We chose to analyze dynamin-related protein 1 (Drp1), because the inactivation of this protein by PKA leads to elongation of mitochondria, whereas its activation leads to mitochondrial fragmentation. PKA performs this regulatory function by phosphorylating serine 656 in rat Drp1 (serine 637 of human Drp1); activation of PKA leads to an approximately doubled phosphorylation level of serine 656 in PC12 cells (40, 49). We therefore asked if Rab32 activity also influences the activity of Drp1. An analysis of lysates using a phospho-Drp1-specific antibody showed that this was indeed the case (Fig. 4*A*). Wild type Rab32 and Rab32T39N increased the Drp1 P656 signal 2- and 2.5-fold, respectively, thus resembling both published Drp1 activation levels and the increases we had observed for phospho-Bad. We could not detect significant changes for the other constructs.

We next analyzed whether the alteration of Drp1 activity coincided with altered Drp1 targeting. Our fractionation protocol that separates heavy and light membranes from the cytosol showed that overexpression of most Rab32 constructs with the exception of Rab32Q85L led to a relative increase of Drp1 on heavy membranes (Fig. 4*B*). Depletion of Rab32 had no effect. Together, our results showed that the activity of Rab32 can modulate the phosphorylation state and the localization of Drp1.

We next asked whether these observations could explain the clustering of fused mitochondria in a perinuclear area when overexpressing Rab32T39N (Fig. 4*C*) and to a lesser extent wild type Rab32 (Fig. 3*A*). To investigate this possibility, we combined the dominant-negative Rab32T39N with the inhibition of PKA. Treatment of transfected cells with the PKA inhibitor H89 led to increased mitochondrial fragmentation, but it was not able to rescue the clustering of mitochondria in the perinuclear area, seen with high expression levels of Rab32T39N (Fig. 4*C*), suggesting that Rab32 affects both mitochondrial mor-

phology and distribution through distinct mechanisms. We next addressed the putative influence of Rab32 on mitochondrial structure and the activity of Drp1 with HeLa cells depleted of Rab32. Similar to the incubation of cells with H89, we saw an increase of mitochondrial fragmentation when we knocked down Rab32 (Fig. 4*D*). This fragmentation of mitochondria could be connected to a roughly 30% decrease of Drp1 phosphorylation, known to lead to hyperactive Drp1 and increased mitochondrial fragmentation (data not shown) (40). We therefore demonstrate that Rab32 controls mitochondrial fission by PKA-mediated inactivation of Drp1. Together, our results show that the manipulation of the expression level and activity of Rab32 leads to a profound change of PKA signaling, mediated by the alteration of PKA localization and resulting in altered activities of the PKA downstream targets Bad and Drp1.

Rab32 Dominant-negative and Dominant-active Constructs Influence the Composition of the MAM—Besides a role for the intracellular distribution of PKA, our immunofluorescence and subcellular fractionation studies (Figs. 1 and 2) suggested that Rab32 could also regulate an ER-associated trafficking step or ER tubule fusion mechanism. From the dual localization of Rab32 to the ER and mitochondria, we hypothesized that Rab32 could specifically affect the MAM, similar to what we had previously described for the cytosolic sorting connector protein PACS-2 (2). To examine this possibility, we compared the composition of the MAM of control HeLa cells with the MAM of HeLa cells that overexpress Rab32 mutants or of HeLa cells that have been depleted of Rab32. We focused on the abundant MAM-enriched chaperone calnexin, of which we detect on average close to 70% of the total signal on the MAM and the remaining amount on membranes of the rough ER (2). We analyzed the MAM localization of calnexin first by immunofluorescence. Cells transfected with an empty plasmid showed a partial overlap of the calnexin and mitochondrial staining patterns as published previously by our laboratory (2). In contrast, cells transfected with a dominant-active form of Rab32 showed reduced but not abolished overlap of these two patterns (Fig. 5*A*). Cells transfected with the dominant-negative Rab32T39N (and to a lesser extent of Rab32 wild type) frequently showed mitochondrial fusion and clustering close to the nucleus (see also Fig. 4*C*), coinciding with a restriction of calnexin/mitochondrial overlap to the perinuclear area. Next, we aimed to understand if any of the Rab32 constructs resulted in a redistribution of calnexin and other MAM markers within the ER. We chose to answer this question by subcellular fractionation, and we analyzed the intra-ER distribution of calnexin. We also ana-

FIGURE 2. **Intracellular localization of FLAG-tagged Rab32 and its GDP/GTP-binding mutants.** *A,* FLAG-tagged Rab32 co-localizes with the ER. HeLa cells were grown on coverslips and transfected with Rab32FLAG wild type. After 48 h, cells were processed for immunofluorescence microscopy. Rab32FLAG was detected with an anti-FLAG monoclonal antibody, calnexin (*CNX*), with our rabbit polyclonal antibody and mitochondria (*Mito*) preloaded with MitoTracker. *Insets* show a magnified area, indicated by *white frames* on the bigger pictures. *Arrowheads* point out Rab32/calnexin/mitochondria triple overlap. *Scale bar,* 25 μm. *B,* FLAG-tagged Rab32Q85L shows reduced overlap with mitochondria. HeLa cells were processed as in *A*. *Arrowheads* point out the absence of the Rab32/calnexin/mitochondria triple overlap. *Scale bar,* 25 μm. *C,* FLAG-tagged Rab32T39N shows overlap with mitochondria that collapse in a perinuclear area. HeLa cells were processed as in *A*. *Arrowheads* point out the Rab32/calnexin/mitochondria triple overlap. *Scale bar,* 25 μm. *D,* Rab32 GDP/GTP binding mutants show distinct fractionation patterns into heavy (*HM*) and light membranes (*LM*) and the cytosol (*Cyt*). Membranes from HeLa cells transfected with Rab32FLAG wild type, Q85L and T39N were fractionated into low and high speed pellets, which were analyzed by Western blot for the FLAG tag. Results from three independent fractionations were quantified. $p = 0.05$ between wild type and Rab32Q85L. *, $p < 0.01$. *E,* Rab32 GDP/GTP binding mutants show distinct ER domain fractionation patterns. Homogenates from HeLa cells transfected with Rab32FLAG wild type (*wt*), Q85L, and T39N were fractionated on a discontinuous 10–30% OptiPrep™ gradient. The presence of FLAG-tagged Rab32 constructs was detected by Western blot. Results from four independent fractionations were quantified. For clarity, error bars were omitted. Additionally, the *graph* on the *right* quantifies the amounts of signal found in fractions 5 and 6 ($p = 0.025$ between Rab32Q85L and Rab32T39N and $p = 0.025$ between wild type and Rab32T39N). tER, transitional ER; *Endo*g, endogenous.
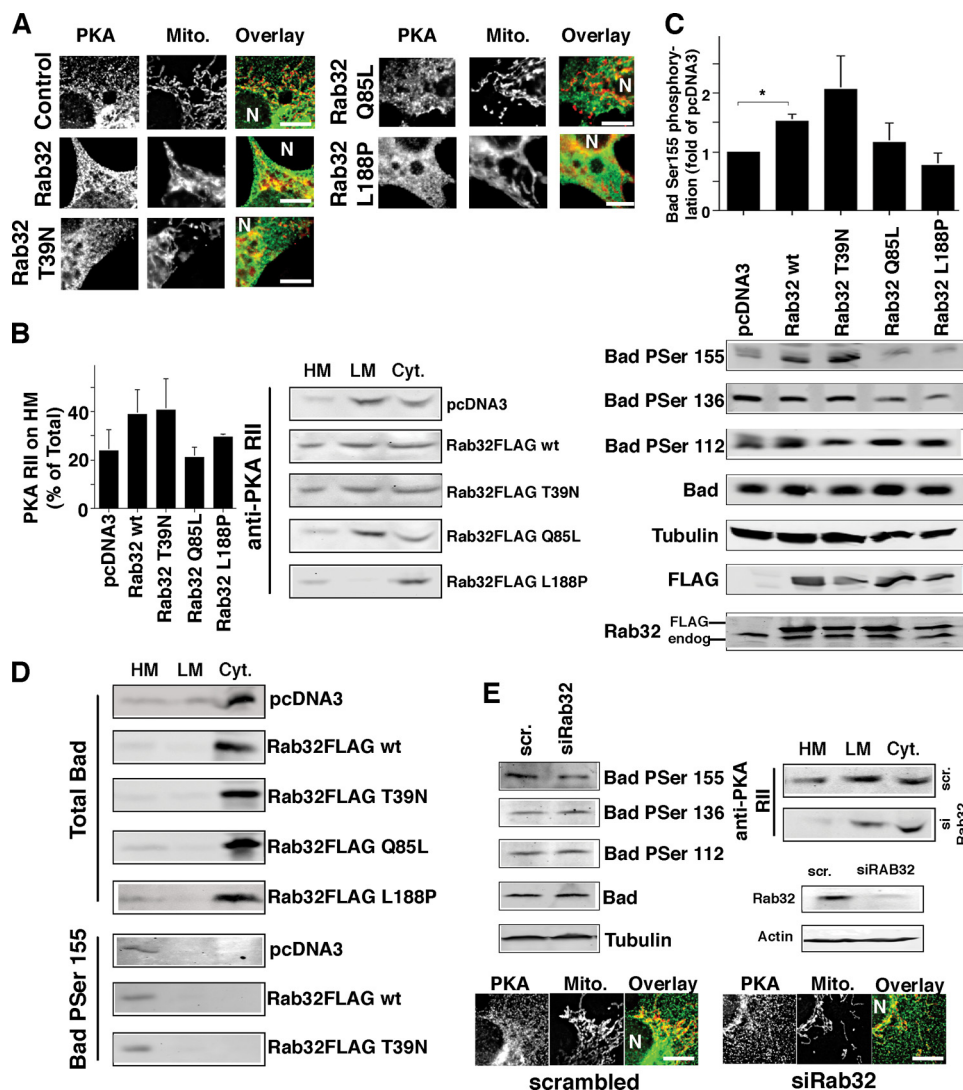
FIGURE 3. **Activity and the expression level of Rab32 affects the intracellular distribution of PKA and its intracellular signaling.** *A,* overlap of PKA with mitochondria (*Mito*) depends on Rab32 activity. HeLa cells were grown on coverslips and transfected with an empty plasmid (pcDNA3) and pcDNA3 containing the cDNA of Rab32FLAG wild type, Rab32FLAG Q85L, Rab32FLAG T39N, and Rab32FLAG L188P. After 48 h, cells were processed for immunofluorescence microscopy, and expressing cells were identified using the FLAG signal (data not shown). PKA RII was detected with a rabbit polyclonal antibody, and mitochondria were preloaded with MitoTracker. Images show portions of cells. The position of the nucleus is indicated by the letter *N. Scale bar,* 10 μm. *B,* distribution of PKA into heavy membranes (*HM*), light membranes (*LM*), and the cytosol (*Cyt*) is modulated by the activity of Rab32. Membranes from HeLa control cells or cells overexpressing Rab32 and Rab32 mutants as indicated were fractionated into low and high speed pellets and the cytosol, which were analyzed by Western blot for PKA RII. *C,* phosphorylation of Bad on serine 155 depends on the expression level and activity of Rab32. HeLa control cells or cells overexpressing Rab32 and Rab32 mutants as indicated were lysed, and lysates were analyzed by Western blot for the presence of Bad phosphorylated on serines 112, 136, and 155, as indicated. Amounts were normalized with the signals for Bad and tubulin, and transfected Rab32 was detected using the FLAG tag of all constructs. $p = 0.025$ between pCDNA3 and wild type Rab32. *D,* distribution of Bad into heavy membranes, light membranes, and the cytosol is not affected by Rab32. Membranes from HeLa control cells or cells overexpressing Rab32 and Rab32 mutants as indicated were fractionated into low and high speed pellets and the cytosol, which were analyzed by Western blot for Bad, and Bad was phosphorylated on serine 155. Note: the information of the Bad serine 155 blots is limited to the localization of this phosphoprotein and not to levels of phosphorylation. *E,* Rab32 expression levels influence Bad serine 155 phosphorylation and PKA localization. *Top left,* analysis of Bad phosphorylation levels of HeLa cells transfected with scrambled (*scr*) siRNA or siRNA for Rab32, analyzed as in *C. Top right,* analysis of PKA membrane distribution in HeLa cells transfected with scrambled siRNA or siRNA (*si*) for Rab32, analyzed as in *B*. Rab32 expression levels are shown in HeLa cells transfected with scrambled siRNA and siRNA for Rab32. *Bottom,* HeLa cells were grown on coverslips and transfected with scrambled siRNA or siRNA for Rab32. After 48 h, cells were processed for immunofluorescence microscopy. PKA RII was detected with a rabbit polyclonal antibody and mitochondria with preloaded with MitoTracker. Images show portions of cells. The position of the nucleus is indicated by the letter *N. Scale bar,* 10 μm.

lyzed mitofusin-2, a marker of the MAM (5), and PDI to assay for the overall proximity of the ER with mitochondria. In HeLa cells that were transfected with dominant-active Rab32Q85L, we detected an even distribution of calnexin between heavy membranes and light membranes, indicative of a relocation of calnexin away from the MAM (Fig. 5*B*). Neither PDI nor mitofusin-2 showed an altered distribution upon Rab32 activation. To further examine this question, we used our OptiPrep™ protocol, because this protocol, but not the classical Percoll protocol, can assay for localization of ER proteins to various membranes of the secretory pathway (Fig. 5*C*). Whereas control cells showed less than 40% of the total amount of calnexin on transitional ER and rER membranes, cells that express Rab32Q85L targeted an additional 30% of calnexin to cellular membranes other than the MAM (Fig. 5*C*). The expression of wild type Rab32 or Rab32T39N had no effect for the calnexin distribution when assayed for either the heavy and light membrane distribution or the OptiPrep™ distribution (Fig. 5, *B* and *C*). We did not detect any increase of the amount of calnexin on the plasma membrane by biotinylation (data not shown), indicating that calnexin is exclusively relocated within the ER upon activation of Rab32. Consistent with the absence of ER or mitochondrial morphology changes, we were unable to detect changes of the localization of PDI, an ER protein that is not enriched on the MAM, or of the mitochondrial MAM marker mitofusin-2, indicating that activation of Rab32 selectively reduces the enrichment of calnexin to the MAM (Fig. 5, *B* and *C*).

We next examined whether the knockdown of Rab32 also affects the distribution of any of the aforementioned markers of the ER and the MAM. Both of our fractionation protocols and our immunofluorescence protocol excluded that possibility (Fig. 5, *D* and *E*) (data not shown). Our results therefore sug-
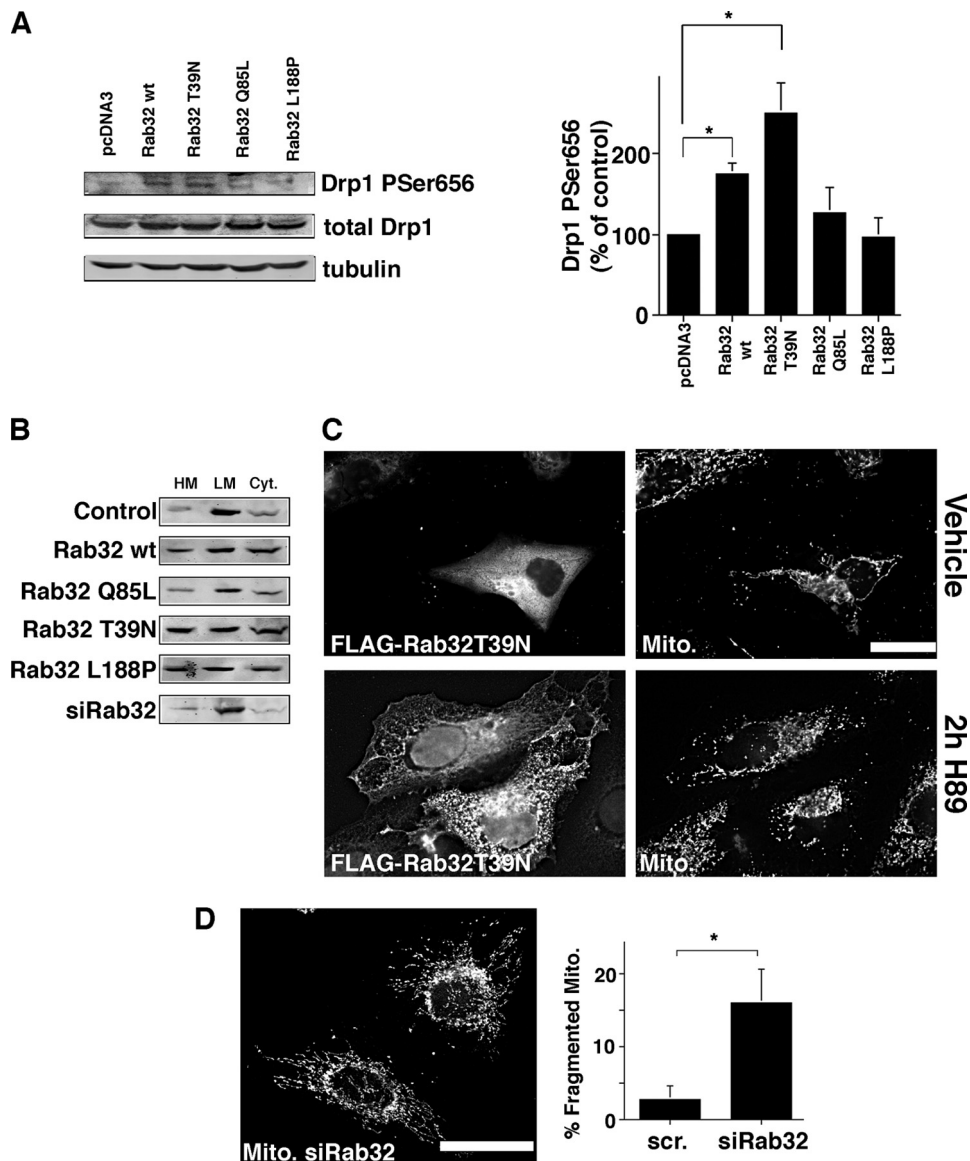
FIGURE 4. **Activity and the expression levels of Rab32 regulate the activity of Drp1.** *A,* phosphorylation of Drp1 on serine 656 depends on the activity of Rab32. HeLa control cells, cells overexpressing Rab32, and Rab32 mutants as indicated were lysed, and lysates were analyzed by Western blot for the presence of Drp1 phosphorylated on serine 656. Amounts were normalized with the signals for total Drp1 and actin, and Drp1 phosphorylated on serine 656 was quantified (*n* = 3). *, *p* < 0.05. *B,* Rab32 does not influence Drp1 targeting. Membranes from HeLa control cells, cells overexpressing Rab32 and Rab32 mutants, or cells where Rab32 has been knocked down as indicated were fractionated into low and high speed pellets and the cytosol, which were analyzed by Western blot for Drp1. *HM,* heavy membranes; *LM,* light membranes; *Cyt,* cytosol. *C,* Rab32 activity and expression levels influence mitochondrial membrane dynamics. *Top row,* expression of Rab32 FLAG T39N leads to the perinuclear clustering of mitochondria as described previously (34). MitoTracker-loaded HeLa cells were transfected with Rab32FLAG T39N, and transfected cells were identified by their positive FLAG signal (*left*). *Bottom row,* cells were transfected and processed as in the *top row* but incubated for 2 h with 10 μM H89. *Scale bar,* 25 μm. *D,* Rab32 knockdown leads to an increase in fragmented mitochondria. HeLa cells transfected with scrambled (*scr*) siRNA (data not shown) or siRNA for Rab32 were loaded with MitoTracker. 10 randomly selected images showing about 50 cells each were quantified for the percentage of cells with fragmented mitochondria (*right*). *p* = 0.025. *Scale bar,* 25 μm.

gest that the activation status of Rab32 but not its expression levels influence the composition of the MAM.

Activity of Rab32 Modulates Apoptosis Onset and ER Calcium Handling—The roles of Rab32 for PKA localization on mitochondria and for the composition of the MAM implicate Rab32 in the regulation of apoptosis onset. Precedents for these connections are AKAP121, the mitochondrial AKAP that blocks apoptosis onset, and PACS-2, the MAM sorting protein

that promotes apoptosis onset (12, 46). We therefore decided to test whether Rab32 similarly plays a role for apoptosis onset. From our results so far, we had determined that Rab32 influences two modifications of Bad known to regulate apoptosis onset; the expression levels of Rab32 influence the PKA-mediated phosphorylation of Bad on serine 155, whereas its activation leads to reduced serine 136 phosphorylation of Bad, known to promote apoptosis. Additionally, Rab32 activation also alters the composition of the MAM that accommodates pro-apoptotic calcium signaling. To further examine the consequences of these observations, we first chose to expose HeLa cells to the tumor necrosis factor-related apoptosis-inducing ligand (TRAIL), because TRAIL is known to depend on the formation of the MAM and also on the action of Bad (27, 50).

We incubated HeLa cells with 500 ng/ml TRAIL, an extrinsic inducer of cell death for 4 h. After this incubation period, cells transfected with an empty plasmid or with scrambled siRNA showed ~20% of cell death when assayed for positive annexin V and propidium iodide staining by flow cytometry (Fig. 6*A*). Consistent with the Bad serine 136/155 and Drp1 serine 656 phosphorylation patterns observed after interference with Rab32 (Fig. 3), the expression of dominant-active FLAG-tagged Rab32Q85L more than doubled the number of dead or dying cells (Fig. 6*A*). In contrast, raising the expression levels of Rab32 by transfection of FLAG-tagged wild type Rab32 halved the number of dead or dying cells, as did the expression of dominant-negative FLAG-tagged Rab32T39N (Fig. 6*A*). Transfection of Rab32L188P or depletion of Rab32 led to an acceler-

ation of apoptosis onset. To confirm and extend these results, we examined the generation of active caspase fragments during TRAIL-induced apoptosis onset in HeLa cells with altered Rab32 expression patterns. We examined early apoptotic events by monitoring the generation of active caspase-8 and late apoptotic events by monitoring generation of active caspase-3. Our results show that the block in apoptosis onset, as seen after Rab32 or Rab32T39N overexpression,
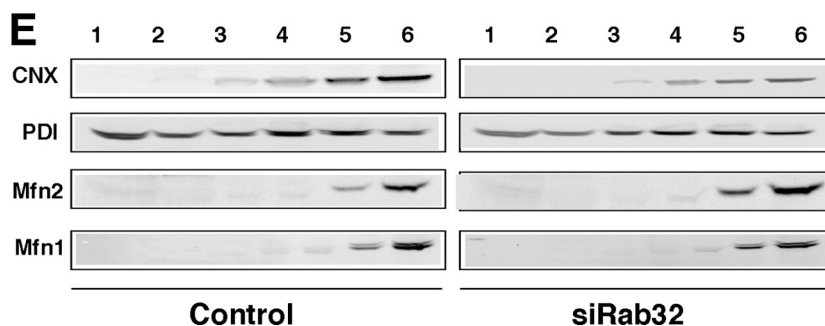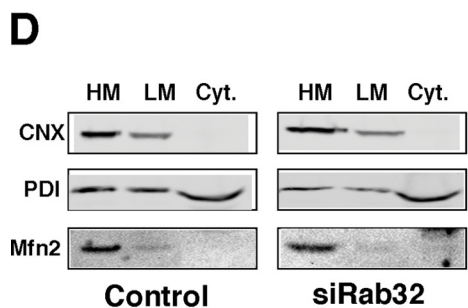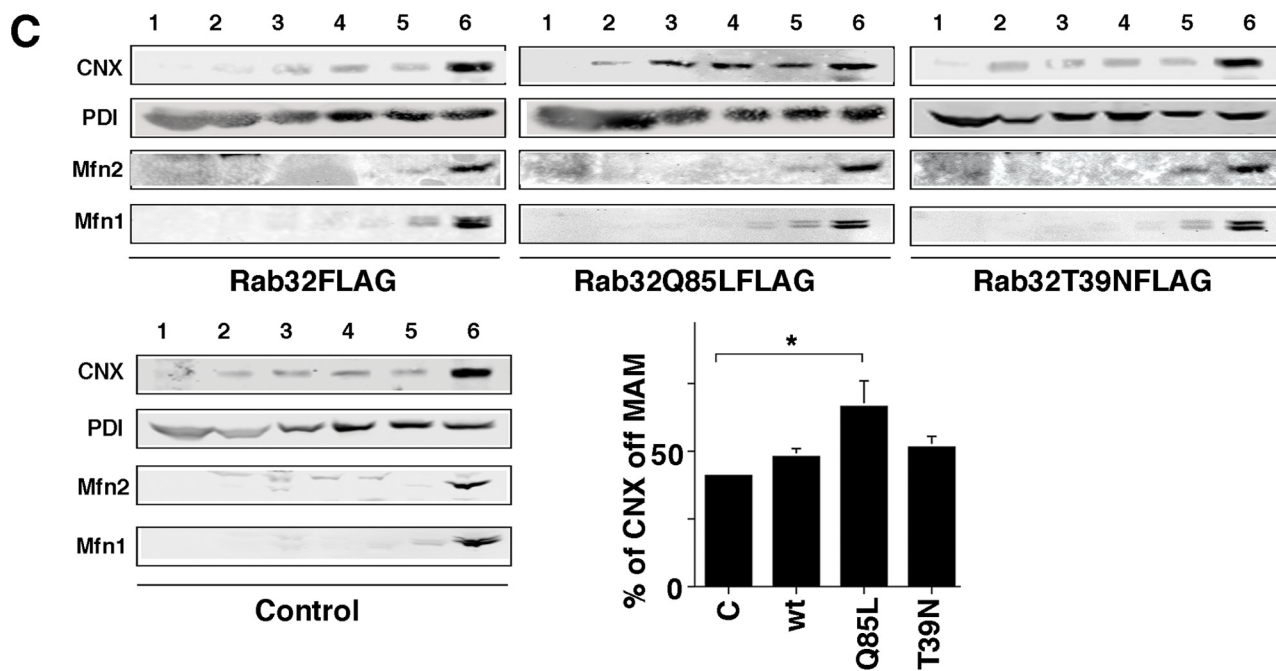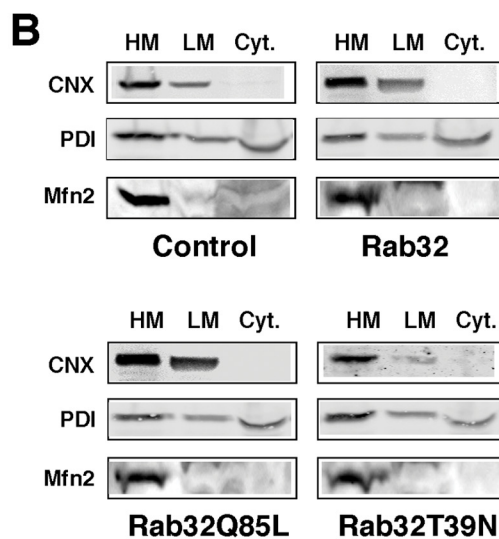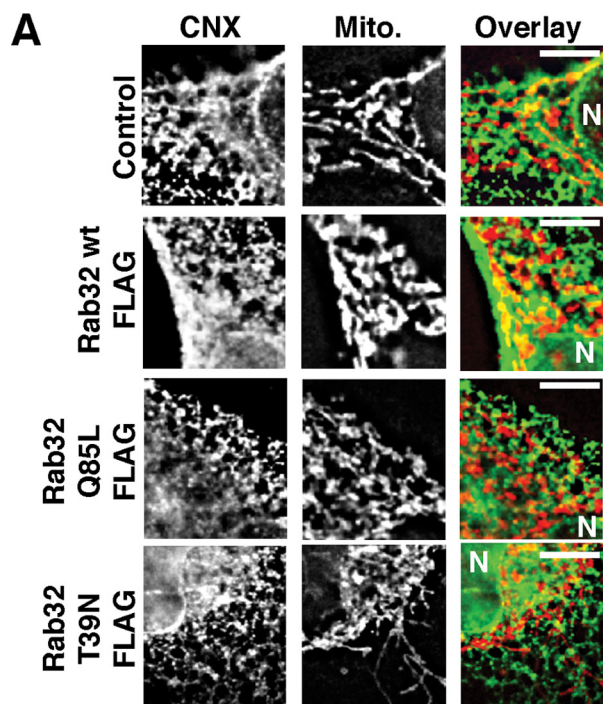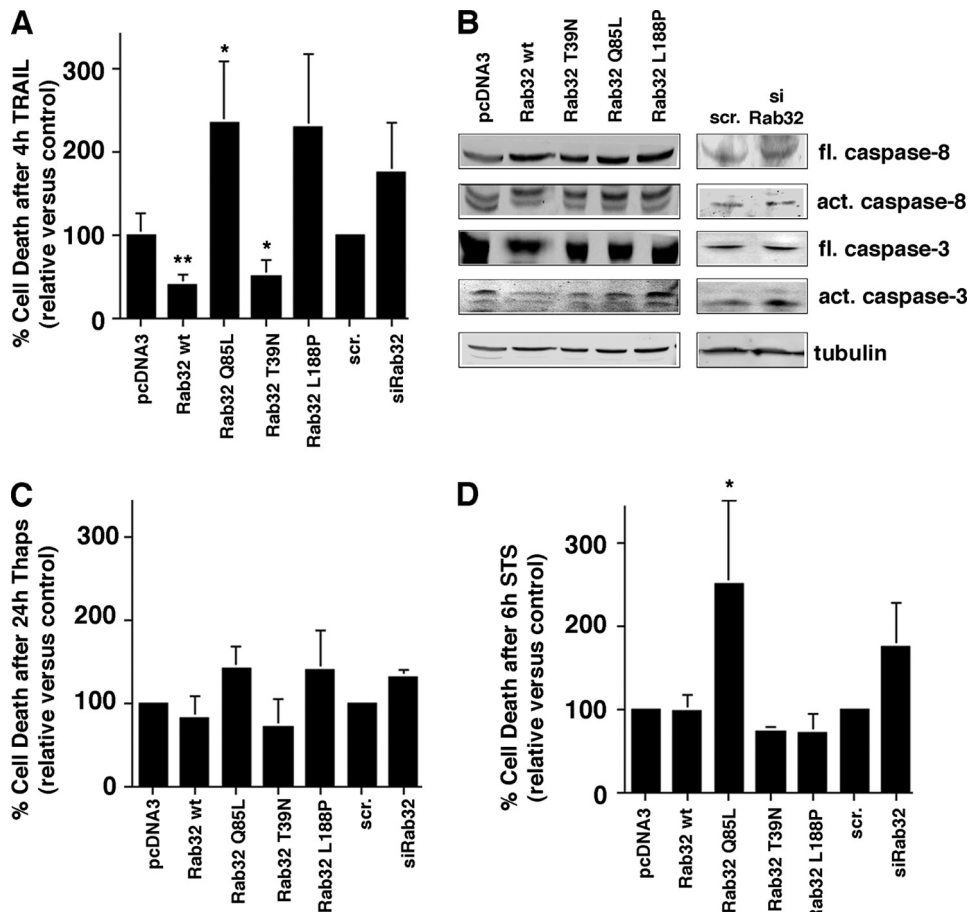
FIGURE 6. **Rab32 influences TRAIL-mediated apoptosis onset.** *A,* apoptosis onset upon TRAIL binding depends on Rab32 activity and expression levels. HeLa cells were transfected with plasmids coding for Rab32 and its GDP/GTP binding mutants and with scrambled (*scr*) or Rab32 siRNA. After 48 h, cells were incubated with 500 ng/ml TRAIL and subsequently analyzed for positive annexin V and propidium iodide signals. The amounts of dead cells were normalized to the vector and scrambled siRNA controls, and results from three independent experiments were graphed. **, $p < 0.005$ for wild type (*wt*); *, $p < 0.01$ for Rab32Q85L and Rab32T39N compared with pcDNA3. *B,* caspase activation upon TRAIL binding depends on Rab32 activity and expression levels. HeLa cells were transfected as in *A*. After 48 h, cells were incubated with 500 ng/ml TRAIL and subsequently analyzed by Western blot for caspases 3 and 8. *fl,* full length; *act,* active. *C,* apoptosis onset upon inhibition of kinases. HeLa cells were transfected with plasmids coding for Rab32 and its GDP/GTP-binding mutants and with scrambled or Rab32 siRNA. After 24 h, cells were incubated with 1 μM thapsigargin for 24 h and subsequently analyzed for positive annexin V and propidium iodide signals. The amounts of dead cells were normalized to the vector, and scrambled siRNA controls and results from three independent experiments were graphed. *D,* apoptosis onset upon staurosporine inhibition of kinases. HeLa cells were transfected with plasmids coding for Rab32 and its GDP/GTP binding mutants and with scrambled or Rab32 siRNA. After 48 h, cells were incubated with 1.2 μM staurosporine for 6 h and subsequently analyzed for positive annexin V and propidium iodide signals. The amounts of dead cells were normalized to the vector and scrambled siRNA controls, and results from three independent experiments were graphed. *, $p < 0.01$ for Rab32Q85L compared with pcDNA3.

coincides with a block in the formation of active caspase-3, but not in a block in the formation of active caspase-8 (Fig. 6*B*). Analogous to our flow cytometry analysis of Rab32 siRNA-transfected cells, Rab32 silencing coincides with the increased formation of active caspase-3 after treatment with TRAIL (Fig. 6*B*).

To further characterize the role of Rab32 in apoptosis onset, we next incubated HeLa cells for 24 h with thapsigargin. Overall, the pattern of apoptosis speed in this scenario resembled the one from TRAIL-induced apoptosis, albeit in a less pronounced way (Fig. 6*C*). Interestingly, when we attempted to recreate a similar effect with the pan-kinase inhibitor staurosporine, we obtained a very different readout, when compared with thapsigargin or TRAIL-induced apoptosis. Although none of the transfections led to protection from apoptosis, the activation of Rab32 (Rab32Q85L) led to a marked increase of apoptosis speed (Fig. 6*D*). This finding confirms that Rab32Q85L does not regulate apoptosis as an AKAP alone, because staurosporine interferes with the activity of PKA, among other kinases (51).

We therefore hypothesized that the Rab32 levels and activation states influence apoptosis in a combination of its distinct properties as an AKAP and as a regulator of MAM composition (Rab32 Q85L) and ER apposition with mitochondria (Rab32 T39N), which could result in altered ER calcium handling (12). To further investigate this possibility, we incubated cells where we had manipulated Rab32

FIGURE 5. **Active Rab32 disrupts the retention of calnexin on the MAM.** *A,* overlap of calnexin (*CNX*) with mitochondria (*Mito*) depends on Rab32 activity. HeLa cells were grown on coverslips and transfected with an empty plasmid (pcDNA3) and pcDNA3 containing the cDNA of Rab32FLAG wild type, Rab32FLAGQ85L, Rab32FLAGT39N, and Rab32FLAGL188P. After 48 h, cells were processed for immunofluorescence microscopy, and expressing cells were identified using the FLAG signal (data not shown). Calnexin was detected with our rabbit polyclonal antibody, and mitochondria were preloaded with MitoTracker. Images show portions of cells. The position of the nucleus is indicated by the letter *N*. Scale bar, 10 μm. *B,* enrichment of calnexin on heavy membranes (*HM*) is disrupted by active Rab32Q85L. Membranes from HeLa control cells or cells overexpressing Rab32 and Rab32 mutants as indicated were fractionated into low and high speed pellets and the cytosol, which were analyzed by Western blot for calnexin. *LM,* light membranes; *Cyt,* cytosol. *C,* active Rab32Q85L disrupts calnexin MAM retention. Homogenates from HeLa cells transfected with Rab32FLAG wild type, Q85L, and T39N were fractionated on a discontinuous 10–30% OptiPrep™ gradient. The presence of calnexin was detected by Western blot. Results from three independent fractionations were quantified, and the amounts of calnexin not found in the MAM fractions 5 and 6 were graphed. $p = 0.05$ between control and Rab32Q85L. *D,* enrichment of calnexin on heavy membranes is not affected by Rab32 knockdown. Membranes were fractionated into low and high speed pellets and the cytosol and probed for calnexin as in *B*. *E,* Rab32 knockdown does not alter the distribution of calnexin on an OptiPrep™ gradient. Homogenates from HeLa cells transfected with scrambled siRNA or Rab32 siRNA were fractionated on a discontinuous 10–30% OptiPrep™ gradient. The presence of calnexin was detected by Western blot.
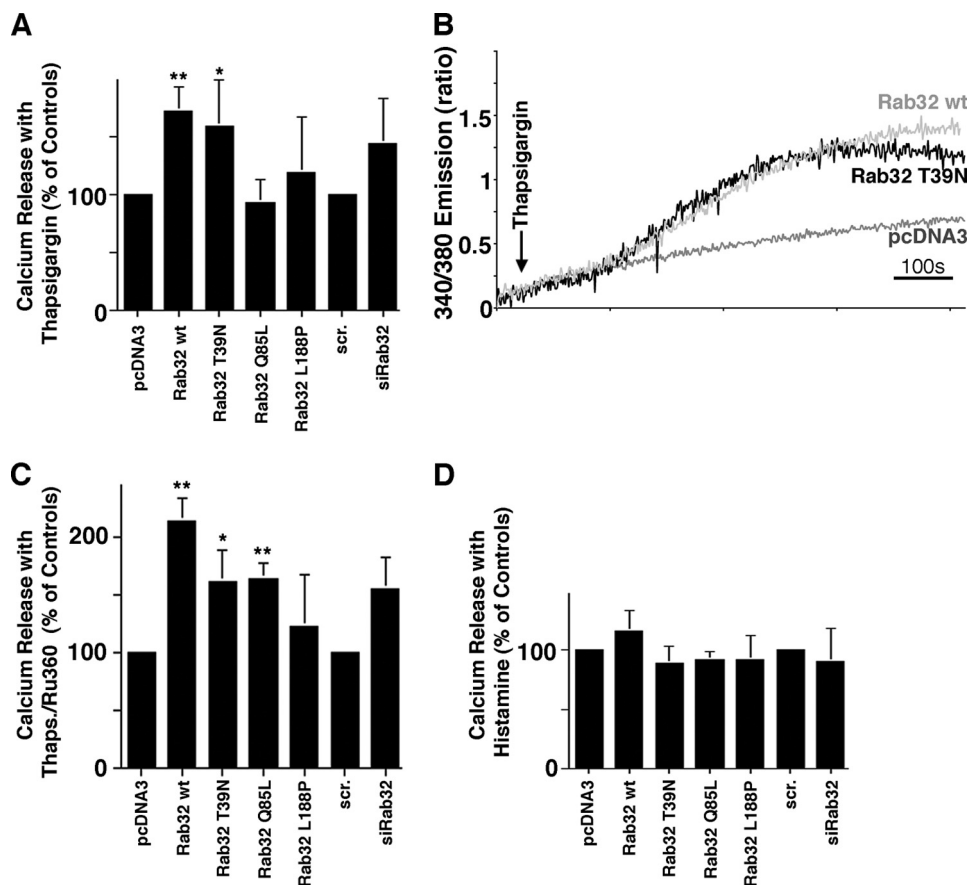
FIGURE 7. **Rab32 affects ER calcium handling.** *A,* thapsigargin-mediated calcium release with altered Rab32 activity and expression levels. HeLa cells were transfected and processed as described under "Experimental Procedures." Calcium was released into the FURA-2-loaded cytosol by the addition of 1 μM thapsigargin. Ratiometric signals were normalized to vector-transfected cells and quantified ($n = 4$). *, $p < 0.05$; **, $p < 0.01$; *scr,* scrambled. *B,* representative calcium release curves for the two constructs showing significant differences. *Curves* are derived from 2×10^6 cells, thus corresponding to an averaged response for these cells. *C,* thapsigargin (*Thaps*)-mediated calcium release with altered Rab32 activity and expression levels in the presence of Ru360. HeLa cells were transfected and processed as in *A* in the presence of 10 μM Ru360 ($n = 4$). *, $p < 0.05$; **, $p < 0.01$. *D,* histamine-mediated calcium release with altered Rab32 activity and expression levels. HeLa cells were transfected and processed as described under "Experimental Procedures." Calcium was released into the FURA-2-loaded cytosol by the addition of 200 μM histamine. Ratiometric signals were normalized to vector-transfected cells and quantified ($n = 3$).

combination of mechanisms. We describe two of these mechanisms. 1) Rab32 modulates ER calcium handling and determines enrichment of calnexin at the MAM. 2) As a PKA-anchoring protein, Rab32 influences the intracellular targeting of PKA, resulting in modulated PKA signaling (Fig. 8). Together, these functions result in a delayed apoptosis onset with high Rab32 levels and accelerated apoptosis with low Rab32 levels. Superimposed on these consequences for apoptosis onset of Rab32 expression levels is the role of the Rab32 activation state. Because dominant-active Rab32 Q85L (but not dominant-negative Rab32 T39N) promotes the onset of apoptosis efficiently (see below), Rab32-mediated apoptosis inhibition following its overexpression has to coincide with low Rab32 activity.

The inhibition of apoptosis onset seen with high Rab32 expression appears to depend largely on its AKAP properties, because an AKAP-deficient Rab32 L188P mutant is unable to delay apoptosis onset. Consistent with this hypothesis, wild type Rab32 promotes Bad phosphorylation on serine 155, a known cause for delayed apoptosis (46). As a consequence, increased Rab32 expression levels may promote glycolysis, regulated by the interplay between Bad and PKA (53). Rab32 also promotes the phosphorylation of Drp1 on serine 656. This phosphorylation is also known to block apoptosis onset, inactivate Drp1, and lead to increased fusion of mitochondria (40). Indeed, overexpressed Rab32T39N and to a lesser extent wild type Rab32 (Figs. 3*A* and 4*C*) cause mitochondria to cluster in a perinuclear area, where they tend to fuse. Because the PKA inhibitor H89 increased mitochondrial fission somewhat in cells overexpressing Rab32T39N, but was unable to reverse mitochondrial clustering, our findings suggest that the two morphological changes depend on distinct functions of Rab32 and cannot be solely attributed to the inactivation of Drp1.

Interestingly, the inhibition of apoptosis with increased Rab32 T39N expression levels coincides with an increased ER calcium release following the administration of thapsigargin (Fig. 7). Higher Rab32 expression levels could promote such an increase by boosting the activity of SERCA, by increasing SERCA expression, or by causing a reduced ability of the ER to transmit calcium to the cytosol and/or the mitochondria. Of these three possibilities, at this point only the third remains, because we observed the reduction of ER/mitochondrial over-

levels or activities with thapsigargin to increase cytosolic calcium through the inhibition of SERCAs in the presence and absence of the mitochondrial calcium uniport inhibitor Ru386 (52). As shown in Fig. 7, *A–C*, thapsigargin led to an increase of cytosolic calcium that was potentiated by overexpression of wild type and dominant-negative Rab32 T39N. Interestingly, in the presence of dominant-active Rab32 Q85L, this increase was only observed when we inhibited mitochondrial calcium import (Fig. 7*C*). Conversely, histamine-induced cytosolic calcium transients do not depend on Rab32, because we could not detect a significantly altered response with either manipulated Rab32 activities or expression levels (Fig. 7*D*). Together, these results demonstrate that Rab32 regulates apoptosis onset from a complex combination of properties, including its identity as an AKAP, and a regulator of MAM properties and calcium handling.

DISCUSSION

Our results implicate Rab32 as a novel regulator of apoptosis onset. Our results also demonstrate that Rab32 is a multifunctional protein that impacts apoptosis onset with a
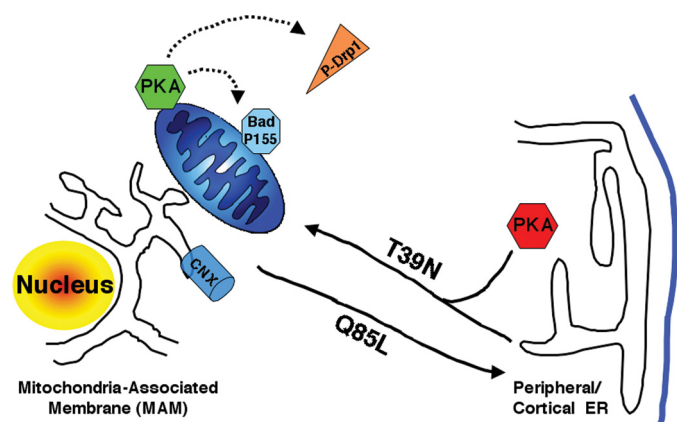
FIGURE 8. **Model for the role of Rab32 in MAM enrichment and PKA localization.** Rab32 regulates the equilibrium between peripheral and perinuclear (MAM) calnexin (*CNX*). Active Rab32 (Q85L) extracts calnexin from the MAM and redistributes it to the cellular periphery. Rab32 also mediates the distribution of PKA between the cellular periphery, where it regulates melanosome biogenesis (43), and the perinuclear area, where it regulates apoptosis onset (this study). Substrates that are PKA-phosphorylated and dependent on Rab32 activity and expression levels include but are not limited to Bad and Drp1.

lap in cells overexpressing Rab32 T39N (34) and to a lesser extent with Rab32 wild type (Fig. 3*A*). In cells expressing these constructs, the mitochondria were collapsed around the nucleus, thus rendering large sections of ER devoid of mitochondria. We could not detect any changes of SERCA2b expression levels for any construct (data not shown).

The most complex phenotype was detected with cells expressing dominant-active Rab32 Q85L that resulted in increased sensitivity to all apoptosis inducers tested. This construct (and the AKAP-disrupted Rab32 L188P) resulted in reduced levels of Bad serine 136 phosphorylation. Moreover and in addition to disrupting calnexin retention on the MAM, active Rab32Q85L also interferes with SERCA calcium handling, when calcium import into the mitochondria was inhibited with Ru360. These cells are therefore very able to transfer calcium from the ER to mitochondria but still exhibit higher calcium concentration within the ER. Hence, dominant-active Rab32 does not disrupt MAMs, as also seen from the distribution of the pan-ER marker PDI and the MAM anchor protein mitofusin-2. Overall, our results suggest that the ER of HeLa cells with high Rab32 expression levels (wild type, T39N, and Q85L) contains more calcium than the ER of control cells. In addition, we found that the efficient transfer of this higher calcium amount to mitochondria requires Rab32 activation (Rab32 Q85L). These characteristics show that Rab32 overexpression results in increased ER calcium levels, similar to PACS-2 and mitofusin-2 depletion, both characterized by a disruption of MAMs as well (5, 12). Contrary to Bcl2 and polycystin-2 overexpression that inhibits apoptosis and lowers ER calcium (54–56), MAM disruption (mediated by Rab32 overexpression or inactivation) is therefore characterized by an increase in ER calcium that coincides with reduced apoptosis progression.

An interesting question is how Rab32 can influence MAM composition. We have summarized our findings in Fig. 8. According to our data, active Rab32 promotes an equilibrated distribution of calnexin between the perinuclear MAM and the

peripheral ER. In principle, other Rab proteins could mediate the opposite effect, *i.e.* the enrichment of ER proteins on the MAM. One candidate could be Rab5 because this Rab protein mediates trafficking at the level of early endosomes (57, 58) but also modulates the morphology of the peripheral ER (32). In analogy to Rab5, Rab32 could influence the MAM by regulating ER tubulation to lead to a polarized structure of the ER. Such a possibility remains to be tested.

The results presented in this paper also show a novel mechanism how members of the Ras-related protein family of Rab proteins could act as oncogenes. Previously, Rabs have been tied to a modulation of cell surface properties, resulting in an increased ability of cancer cells to metastasize (59, 60). Intriguingly, high levels of Rab32 correlate frequently with high levels of Bad phosphorylated on serine 155 in melanoma tissue, melanoma cell lines, and breast cancer tissue (data not shown). A full description of the role of Rab32 in apoptosis and tumorigenesis can, however, not rely on the sole analysis of its expression levels, but rather it requires the understanding of the upstream regulation of its activity, in particular the identification of the Rab32 GDP dissociation inhibitor displacement factor and of the Rab32 guanine nucleotide exchange factor. Additional complexity is added by PKA regulatory subunits that modulate PKA activity and thus potentially the functions of Rab32. Rab32 therefore emerges as a complex apoptosis regulator whose role can be modulated on at least two levels as follows: its expression levels that correlate with anti-apoptotic PKA signaling, and its activity levels that control MAM composition and ER calcium handling.

REFERENCES

1. Vance, J. E. (1990) *J. Biol. Chem.* **265,** 7248–7256
2. Myhill, N., Lynes, E. M., Nanji, J. A., Blagoveshchenskaya, A. D., Fei, H., Carmine Simmen, K., Cooper, T. J., Thomas, G., and Simmen, T. (2008) *Mol. Biol. Cell* **19,** 2777–2788
3. Pinton, P., Giorgi, C., Siviero, R., Zecchini, E., and Rizzuto, R. (2008) *Oncogene* **27,** 6407–6418
4. Hayashi, T., Rizzuto, R., Hajnoczky, G., and Su, T. P. (2009) *Trends Cell Biol.* **19,** 81–88
5. de Brito, O. M., and Scorrano, L. (2008) *Nature* **456,** 605–610
6. Rizzuto, R., Pinton, P., Carrington, W., Fay, F. S., Fogarty, K. E., Lifshitz, L. M., Tuft, R. A., and Pozzan, T. (1998) *Science* **280,** 1763–1766
7. Rizzuto, R., Brini, M., Murgia, M., and Pozzan, T. (1993) *Science* **262,** 744–747
8. Filippin, L., Magalhães, P. J., Di Benedetto, G., Colella, M., and Pozzan, T. (2003) *J. Biol. Chem.* **278,** 39224–39234
9. Brostrom, M. A., and Brostrom, C. O. (2003) *Cell Calcium* **34,** 345–363
10. Michalak, M., Robert Parker, J. M., and Opas, M. (2002) *Cell Calcium* **32,** 269–278
11. Boehning, D., Patterson, R. L., Sedaghat, L., Glebova, N. O., Kuroaki, T., and Snyder, S. H. (2003) *Nat. Cell Biol.* **5,** 1051–1061
12. Simmen, T., Aslan, J. E., Blagoveshchenskaya, A. D., Thomas, L., Wan, L., Xiang, Y., Feliciangeli, S. F., Hung, C. H., Crump, C. M., and Thomas, G. (2005) *EMBO J.* **24,** 717–729
13. Laude, A. J., and Simpson, A. W. (2009) *FEBS J.* **276,** 1800–1816
14. Higo, T., Hattori, M., Nakamura, T., Natsume, T., Michikawa, T., and

Mikoshiba, K. (2005) *Cell* **120,** 85–98

15. Roderick, H. L., Lechleiter, J. D., and Camacho, P. (2000) *J. Cell Biol.* **149,** 1235–1248

16. Li, Y., and Camacho, P. (2004) *J. Cell Biol.* **164,** 35–46

17. John, L. M., Lechleiter, J. D., and Camacho, P. (1998) *J. Cell Biol.* **142,** 963–973

18. Li, G., Mongillo, M., Chin, K. T., Harding, H., Ron, D., Marks, A. R., and Tabas, I. (2009) *J. Cell Biol.* **186,** 783–792

19. Gilady, S. Y., Bui, M., Lynes, E. M., Benson, M. D., Watts, R., Vance, J. E., and Simmen, T. (2010) *Cell Stress Chaperones* **15,** 619–629

20. Csordás, G., Renken, C., Várnai, P., Walter, L., Weaver, D., Buttle, K. F., Balla, T., Mannella, C. A., and Hajnóczky, G. (2006) *J. Cell Biol.* **174,** 915–921

21. Osibow, K., Frank, S., Malli, R., Zechner, R., and Graier, W. F. (2006) *Biochem. J.* **396,** 173–182

22. Simmen, T., Lynes, E. M., Gesson, K., and Thomas, G. (2010) *Biochim. Biophys. Acta* **1798,** 1465–1473

23. Kornmann, B., Currie, E., Collins, S. R., Schuldiner, M., Nunnari, J., Weissman, J. S., and Walter, P. (2009) *Science* **325,** 477–481

24. Boldogh, I. R., Nowakowski, D. W., Yang, H. C., Chung, H., Karmon, S., Royes, P., and Pon, L. A. (2003) *Mol. Biol. Cell* **14,** 4618–4627

25. Szabadkai, G., Bianchi, K., Várnai, P., De Stefani, D., Wieckowski, M. R., Cavagna, D., Nagy, A. I., Balla, T., and Rizzuto, R. (2006) *J. Cell Biol.* **175,** 901–911

26. Youker, R. T., Shinde, U., Day, R., and Thomas, G. (2009) *Biochem. J.* **421,** 1–15

27. Aslan, J. E., You, H., Williamson, D. M., Endig, J., Youker, R. T., Thomas, L., Shu, H., Du, Y., Milewski, R. L., Brush, M. H., Possemato, A., Sprott, K., Fu, H., Greis, K. D., Runckel, D. N., Vogel, A., and Thomas, G. (2009) *Mol. Cell* **34,** 497–509

28. Turner, M. D., Plutner, H., and Balch, W. E. (1997) *J. Biol. Chem.* **272,** 13479–13483

29. Jordens, I., Marsman, M., Kuijl, C., and Neefjes, J. (2005) *Traffic* **6,** 1070–1077

30. Grosshans, B. L., Ortiz, D., and Novick, P. (2006) *Proc. Natl. Acad. Sci. U.S.A.* **103,** 11821–11827

31. Ozeki, S., Cheng, J., Tauchi-Sato, K., Hatano, N., Taniguchi, H., and Fujimoto, T. (2005) *J. Cell Sci.* **118,** 2601–2611

32. Audhya, A., Desai, A., and Oegema, K. (2007) *J. Cell Biol.* **178,** 43–56

33. Frederick, R. L., Okamoto, K., and Shaw, J. M. (2008) *Genetics* **178,** 825–837

34. Alto, N. M., Soderling, J., and Scott, J. D. (2002) *J. Cell Biol.* **158,** 659–668

35. Michel, J. J., and Scott, J. D. (2002) *Annu. Rev. Pharmacol. Toxicol.* **42,** 235–257

36. Feliciello, A., Gottesman, M. E., and Avvedimento, E. V. (2001) *J. Mol. Biol.* **308,** 99–114

37. Beene, D. L., and Scott, J. D. (2007) *Curr. Opin. Cell Biol.* **19,** 192–198

38. Livigni, A., Scorziello, A., Agnese, S., Adornetto, A., Carlucci, A., Garbi, C., Castaldo, I., Annunziato, L., Avvedimento, E. V., and Feliciello, A. (2006) *Mol. Biol. Cell* **17,** 263–271

39. Carlucci, A., Lignitto, L., and Feliciello, A. (2008) *Trends Cell Biol.* **18,** 604–613

40. Cribbs, J. T., and Strack, S. (2007) *EMBO Rep.* **8,** 939–944

41. Cohen-Solal, K. A., Sood, R., Marin, Y., Crespo-Carbone, S. M., Sinsimer, D., Martino, J. J., Robbins, C., Makalowska, I., Trent, J., and Chen, S. (2003) *Biochim. Biophys. Acta* **1651,** 68–75

42. Bao, X., Faris, A. E., Jang, E. K., and Haslam, R. J. (2002) *Eur. J. Biochem.* **269,** 259–271

43. Wasmeier, C., Romao, M., Plowright, L., Bennett, D. C., Raposo, G., and Seabra, M. C. (2006) *J. Cell Biol.* **175,** 271–281

44. Park, M., Serpinskaya, A. S., Papalopulu, N., and Gelfand, V. I. (2007) *Curr. Biol.* **17,** 2030–2034

45. Stone, S. J., and Vance, J. E. (2000) *J. Biol. Chem.* **275,** 34534–34540

46. Affaitati, A., Cardone, L., de Cristofaro, T., Carlucci, A., Ginsberg, M. D., Varrone, S., Gottesman, M. E., Avvedimento, E. V., and Feliciello, A. (2003) *J. Biol. Chem.* **278,** 4286–4294

47. Datta, S. R., Dudek, H., Tao, X., Masters, S., Fu, H., Gotoh, Y., and Greenberg, M. E. (1997) *Cell* **91,** 231–241

48. Lizcano, J. M., Morrice, N., and Cohen, P. (2000) *Biochem. J.* **349,** 547–557

49. Chang, C. R., and Blackstone, C. (2007) *J. Biol. Chem.* **282,** 21583–21587

50. Kang, Y. C., Kim, K. M., Lee, K. S., Namkoong, S., Lee, S. J., Han, J. A., Jeoung, D., Ha, K. S., Kwon, Y. G., and Kim, Y. M. (2004) *Cell Death Differ.* **11,** 1287–1298

51. Tamaoki, T. (1991) *Methods Enzymol.* **201,** 340–347

52. Matlib, M. A., Zhou, Z., Knight, S., Ahmed, S., Choi, K. M., Krause-Bauer, J., Phillips, R., Altschuld, R., Katsube, Y., Sperelakis, N., and Bers, D. M. (1998) *J. Biol. Chem.* **273,** 10223–10231

53. Danial, N. N., Gramm, C. F., Scorrano, L., Zhang, C. Y., Krauss, S., Ranger, A. M., Datta, S. R., Greenberg, M. E., Licklider, L. J., Lowell, B. B., Gygi, S. P., and Korsmeyer, S. J. (2003) *Nature* **424,** 952–956

54. Foyouzi-Youssefi, R., Arnaudeau, S., Borner, C., Kelley, W. L., Tschopp, J., Lew, D. P., Demaurex, N., and Krause, K. H. (2000) *Proc. Natl. Acad. Sci. U.S.A.* **97,** 5723–5728

55. Pinton, P., Ferrari, D., Magalhães, P., Schulze-Osthoff, K., Di Virgilio, F., Pozzan, T., and Rizzuto, R. (2000) *J. Cell Biol.* **148,** 857–862

56. Wegierski, T., Steffl, D., Kopp, C., Tauber, R., Buchholz, B., Nitschke, R., Kuehn, E. W., Walz, G., and Köttgen, M. (2009) *EMBO J.* **28,** 490–499

57. Gorvel, J. P., Chavrier, P., Zerial, M., and Gruenberg, J. (1991) *Cell* **64,** 915–925

58. Chavrier, P., Parton, R. G., Hauri, H. P., Simons, K., and Zerial, M. (1990) *Cell* **62,** 317–329

59. Cheng, K. W., Lahad, J. P., Kuo, W. L., Lapuk, A., Yamada, K., Auersperg, N., Liu, J., Smith-McCune, K., Lu, K. H., Fishman, D., Gray, J. W., and Mills, G. B. (2004) *Nat. Med.* **10,** 1251–1256

60. Cheng, K. W., Lahad, J. P., Gray, J. W., and Mills, G. B. (2005) *Cancer Res.* **65,** 2516–2519